

Properties of ferroelectric nanodots

embedded in a polarizable medium: Atomistic simulations

S. Prosandeev^{1,2} and L. Bellaiche¹

¹*Physics Department, University of Arkansas, Fayetteville, AR 72701*

²*Institute of Physics, Rostov State University, Rostov on Don, Russia 344090*

(Dated: October 24, 2018)

Abstract

An atomistic approach is used to investigate finite-temperature properties of ferroelectric nanodots that are embedded in a polarizable medium. Different phases are predicted, depending on the ferroelectric strengths of the material constituting the dot and of the system forming the medium. In particular, novel states, exhibiting a coexistence between two kinds of order parameters or possessing a peculiar order between dipole vortices of adjacent dots, are discovered. We also discuss the origins of these phases, e.g. depolarizing fields and medium-driven interactions between dots.

Ferroelectric nanostructures (FENs) are of current high interest, because of their technological promise in leading toward miniaturized devices¹, and because of their potential in resulting in new phenomena. For instance, it was recently predicted that *isolated* nanodots of ferroelectrics can have a vortex structure for their dipoles below a critical temperature^{2,3,4}. Such vortex does not create any polarization but rather generates a macroscopic toroidal moment, that involves the cross product between the \mathbf{r}_i vectors locating the i unit cells and their local electrical dipoles \mathbf{p}_i – i.e., it is defined as $\mathbf{G} = \frac{1}{2N} \sum_i \mathbf{r}_i \times \mathbf{p}_i$, where the sum runs over the N unit cells of the nanodot. Being able to switch the direction of \mathbf{G} opens exciting opportunities for nanomemory devices^{2,5}.

Interestingly, the possibility for the dipoles to form a vortex structure has been omitted in the previous studies (see, e.g., Refs.^{6,7,8} that used an effective medium approximation) aimed in determining the properties of ferroelectric or paraelectric nanoparticles that are *embedded* in a polarizable medium. As a result, original features may have been overlooked in these composite systems. For instance, one may wonder if novel states occur in such two-component materials. In particular, can dipole vortices in dots immersed in a polarizable medium coexist with a spontaneous polarization (unlike in isolated dots^{2,3})? Similarly, how do toroidal moments of neighboring dots organize themselves? (e.g, are they lying along parallel or antiparallel directions?). It would also be worthwhile to determine the dependency of these novel states (if any) on the ferroelectrics strengths of the materials forming the dot and medium, and to reveal their governing mechanisms. The aim of this Letter is to address the issues mentioned above, by performing atomistic simulations.

Our atomistic scheme is based on the construction of an effective Hamiltonian, with the total energy E being written as a sum of two main terms,

$$E(\{\mathbf{u}_i\}, \{\eta_H\}, \{\eta_I\}, \{\sigma_j\}) = E_{\text{ave}}(\{\mathbf{u}_i\}, \{\eta_H\}, \{\eta_I\}) + E_{\text{loc}}(\{\mathbf{u}_i\}, \{\eta_I\}), \quad (1)$$

where E_{ave} – as in Refs.^{9,10} – is the total energy associated with the hypothetical *simple* $A < B > O_3$ system resulting from the use of the virtual crystal approximation (VCA)¹¹ to mimic $A(B', B'')O_3$ compounds; E_{loc} gathers alloying terms going beyond the VCA approximation; \mathbf{u}_i is the local soft mode (directly related to the electrical dipole) in unit cell i ; $\{\eta_H\}$ and $\{\eta_I\}$ are the *homogeneous* and *inhomogeneous* strain tensor, respectively¹²; $\{\sigma_j\}$ characterizes the atomic configuration, that is, $\sigma_j = 1$ (resp. -1) if there is a B' (resp. B'') cation at the B-lattice site j of the $A(B', B'')O_3$ materials. For E_{ave} , we use the analytical expression

proposed in Ref.¹² for *simple* ABO₃ systems. For E_{loc} , we use the following expression:

$$E_{\text{loc}}(\{\mathbf{u}_i\}, \{\eta_I\}, \{\sigma_j\}) = \sum_{ij} [Q_{j,i}\sigma_j \mathbf{e}_{ji} \cdot \mathbf{u}_i + R_{j,i}\sigma_j \mathbf{f}_{ji} \cdot \mathbf{v}_i] + \sum_i \Delta\kappa(\sigma_i) u_i^2 \quad (2)$$

where the sums over i and j run over unit cells and mixed sublattice sites, respectively. $\{\mathbf{v}_i\}$ are dimensionless local displacements which are related to the inhomogeneous strain variables inside each cell¹². $Q_{j,i}(\sigma_j)$ and $R_{j,i}(\sigma_j)$ characterize the strengths of the alloying-induced intersite interactions. \mathbf{e}_{ji} is a unit vector joining the site j to the center of the soft-mode vector \mathbf{u}_i , and \mathbf{f}_{ji} is a unit vector joining the site j to the origin of the displacement \mathbf{v}_i . Practically, we included contributions up to the third neighbors for $Q_{j,i}(\sigma_j)$, and over the first-neighbor shell for $R_{j,i}(\sigma_j)$. Note that, for systems made of AB''O₃ dots embedded in a AB'O₃ medium, these contributions only play a role near the dots' surfaces – because of the analytical expression of the first two terms of Eq. (2). The last term of Eq. (2), which involves the $\Delta\kappa(\sigma_i)$ parameters, characterizes the onsite contribution of alloying. It is an original contribution since it was not included in the alloy effective Hamiltonians of Refs.^{9,10}. We incorporate such term here – which is consistent with first-principles results of Ref.¹³ – because it provides an easy way to artificially adjust the “ferroelectric strength” of AB'O₃ and AB''O₃ simple systems, by playing with the $\Delta\kappa(\sigma_i = +1)$ and $\Delta\kappa(\sigma_i = -1)$ parameters. For instance, a large negative (respectively, positive) $\Delta\kappa(\sigma_i = -1)$ leads to a strong ferroelectric instability (respectively, no ferroelectric instability) of the pure AB''O₃ material. In the following, we will denote $\Delta\kappa$ as the difference between the two alloying-onsite parameters, i.e. $\Delta\kappa = \Delta\kappa(\sigma_i = +1) - \Delta\kappa(\sigma_i = -1)$. At the exceptions of the adjustable $\Delta\kappa(\sigma_i = +1)$ and $\Delta\kappa(\sigma_i = -1)$ variables, all the parameters of our toy model described by Eqs. (1)-(2) are those derived for the Pb(Zr_{0.5}Ti_{0.5})O₃ solid solution from first-principles calculations⁹. [Such parameters yield a tetragonal ferroelectric ground-state with a polarization pointing along a $\langle 001 \rangle$ direction and a Curie temperature $\simeq 1000$ K, in the Pb(Zr_{0.5}Ti_{0.5})O₃ bulk]. As a result, we numerically found that $\Delta\kappa(\sigma_i = +1)$ or $\Delta\kappa(\sigma_i = -1)$ $\simeq +0.0094$ a.u. is the highest value to have a ferroelectric ground-state in pure AB'O₃ or AB''O₃ material, respectively.

The total energy of Eq. (1) is used in Monte-Carlo simulations to obtain the local mode vectors, the toroidal moment of polarization and the homogeneous strain tensor $\{\eta_H\}$ at different temperatures. Typically, 2×10^4 Monte-Carlo sweeps are first performed to equilibrate the system, and then 8×10^4 sweeps are used to get various statistical averages. The

temperature is decreased in small steps down to 1 K. We also heat up the investigated systems by small temperature steps from 1 K, to look for thermal hysteresis. We also computed the dielectric susceptibility, as well as the toroidal susceptibility (which characterizes the response of the toroidal moment to the curl of the electric field¹⁴), as in Ref.¹⁵.

Figure 1 shows the temperature-versus- $\Delta\kappa$ phase diagram of a $16 \times 16 \times 16$ periodic supercell (20480 atoms, 64Å lateral size) containing an $AB''O_3$ cubic dot of 48Å of lateral dimension embedded in a host matrix made of pure $AB'O_3$. Practically, for *positive* $\Delta\kappa$, $\Delta\kappa(\sigma_i = -1)$ is set to zero while $\Delta\kappa(\sigma_i = +1)$ is allowed to vary. These cases thus correspond to a specific ferroelectric dot immersed in different media that are all ferroelectrically-harder than the dot and that can either be ferroelectric (small positive $\Delta\kappa$) or paraelectric (larger positive $\Delta\kappa$). The reverse situation applies for the case of *negative* $\Delta\kappa$: $\Delta\kappa(\sigma_i = -1)$ is varied while $\Delta\kappa(\sigma_i = +1)$ vanishes, implying that we mimic either ferroelectric dots with smaller ferroelectricity strength than the medium (for small negative $\Delta\kappa$) or paraelectric dots (for larger negative $\Delta\kappa$) inserted in a matrix made from a specific ferroelectric material.

Figure 1 reveals the existence of six different phases, for which the associated dipole patterns are displayed in insets [Phase boundaries were practically determined by identifying the peak or abrupt jumps of the susceptibilities altogether with the appearance of the spontaneous polarization or toroidal moment. Note that, in principle, further study could reveal some of these features to be associated with continuous changes in configuration rather than true phase boundaries *per se*. However, some preliminary results obtained by us on the basis of the finite-size scaling analysis¹⁶ do confirm the existence of true phase transitions.] Two of these phases are expected based on previous knowledge of ferroelectrics: the paraelectric, PE, state at high temperature, and the ferroelectric, FE1, phase occurring at intermediate and low temperature when $\Delta\kappa$ is small in magnitude. In this FE1 state, both the dot and medium develop homogeneous parallel dipoles – with these dipoles being larger (resp., smaller) in the dot than in the host when $\Delta\kappa$ is positive (resp., negative), as consistent with our definition of $\Delta\kappa$ (i.e., the difference between the onsite parameters of the medium and the dot).

Four phases of Fig. 1 can be considered as novel structures. They are denoted as FT, FE1+FT, FE2 and FE3, respectively. The FT phase, which occurs for the largest positive $\Delta\kappa$ values, exhibits a finite toroidal moment. The appearance of this state in this region of the phase diagram results from the fighting of the dipoles in the dot against the large

enough depolarizing field^{2,3,4} (which arises from the significant non-similarity between the “more ferroelectric” dot and “less ferroelectric” host material). The present discovery of this FT phase is, in fact, consistent with the previous finding that *isolated* ferroelectric dots surrounded by vacuum exhibit a vortex structure for their dipoles below a critical temperature^{2,3,4}, because one can think of vacuum as a medium having an infinite positive value for $\Delta\kappa(\sigma_i = +1)$. However and unlike in the vacuum, the dipoles of the host matrix in the FT phase become slightly polarized by the nearby dipoles located inside the dots and near the surfaces, when this host matrix is still rather “soft” (see corresponding inset of Fig.1). For such cases, the medium thus also generates a toroidal moment that is parallel to, but of lower magnitude than, the one solely associated with the dot.

Moreover, the FE1+FT phase appearing in the phase diagram at small temperature and within a narrow range of positive $\Delta\kappa$ is rather remarkable because it displays an unusual cohabitation between the toroidal moment and the spontaneous polarization. In this phase, the medium generates an electric field inside the dot, that (as in some magnetic nanodots under an external magnetic field¹⁷ or in some ferroelectric dots subject to electric fields¹⁸) leads to the shift of the vortex structure with respect to the center of the dot (see the corresponding inset in Fig. 1) and thus activates a polarization. Note, too, that this FE1+FT phase can be considered as a low-temperature bridging structure between the FE1 and FT phases since we numerically found that the FE1-to-FE1+FT and FE1+FT-to-FT transitions are second-order in character, unlike the FT-to-FE1 phase transition that displays all the expected features of a first-order phase transition (e.g., the toroidal moment suddenly disappears at this boundary in favor of a *finite* value of the polarization, and the FT-to-FE1 boundary line has a rather large thermal hysteresis: it is typically increased by $\simeq 100$ K with respect to the one displayed in Fig. 1 when heating, rather than cooling).

The last two phases, FE2 and FE3, appearing in Fig. 1 are both ferroelectric and occur at intermediate and low temperatures, respectively, for the largest negative values of $\Delta\kappa$. In other words, these two states correspond to cases for which the dot, unlike the medium, is made of a material that desires to be paraelectric. As a result, the FE2 phase exhibits a spontaneous polarization that originates from the alignment along a $\langle 001 \rangle$ direction of dipoles belonging to some *specific regions of the medium*. More specifically, these regions belong to the $\{001\}$ planes that contain the polarization direction and that do not possess any site belonging to the dot (see, e.g, the corresponding inset of Fig. 1 for FE2 showing the

homogeneity of dipoles in the top and bottom planes, while the parts of the medium located at the right and left sides of the dot do *not* display any homogeneity for their dipoles). The reason behind such unique arrangement, in which the largest dipoles in the medium intentionally avoid to point towards the dots, is once again the minimization of the depolarizing energy. When decreasing the temperature, the FE2 phase transforms into the FE3 state, that is associated with a polarization that has now two non-vanishing components along two different $\langle 001 \rangle$ directions. More precisely, the corresponding inset of Fig. 1 reveals that, in the FE3 phase, the top and bottom parts of the medium exhibit dipoles that are similar in direction than those in the FE2 phase, while dipoles located in the medium at the right and left sides of the dot have dipoles aligned along a *perpendicular* direction. Such dipole arrangement arises, once again, from a minimization of the depolarizing energy. Interestingly, the FE2 and FE3 phases bear resemblance to some states that were experimentally found recently in artificially constructed magnets¹⁹. Moreover, note that we numerically found that another solution (but of slightly higher energy than that of the FE3 phase) is possible at low temperature for large negative $\Delta\kappa$: it consists of the top and bottom parts of the medium having dipoles homogeneously aligned a specific $\langle 001 \rangle$ directions (as in the FE2 phase) while the dipoles of the medium located at the right and left sides of the dot form a vortex structure.

We also numerically checked that all the phases of Fig. 1 still occur when varying the size of the dot or the size of the whole supercell. Moreover, out of these six states, the FT and FE1+FT phases are the soles structures that refine themselves when allowing *several* $AB''O_3$ dots to be present in a supercell possessing a $AB'O_3$ medium. More precisely, Figs 2 show that, for large enough positive $\Delta\kappa$, neighboring dots have vortices rotating in an *opposite* fashion. In other words, the FT (respectively, the FE1+FT) phase of Fig.1 should in fact become the AFT (respectively, FE1+AFT) structure of Fig. 2a (respectively, Fig. 2b) when dots are close enough from each other (as in dots' arrays). Such novel *antiferrotoric* phases, unlike the FT and FT+FE1 states, allow the dipoles located *between* two adjacent dots to all point along similar directions, which minimizes the corresponding domain wall energy at the cost of the electrostatic interaction between neighboring vortices (we numerically found that the direct electrostatic interaction between two different toroidal moments should align these moments along the same direction – that is, it should lead to a ferrotoric, rather than antiferrotoric, order). Furthermore, Fig. 2b reveals that the centers of the vortices in the

FE1+AFT phase form a rather unusual lattice (see, e.g., that the centers of the vortices have different y -locations for dots that are adjacent along the x -axis). This unique geometry originates from the desire of the whole system to maximize the number of its dipoles (in the dots) lying along the polarization direction, considering the underlying antiferrotoric order.

In summary, varying the polarizabilities of the embedded dots and of the medium opens a new way for engineering dipole patterns. The fundamental reasons behind such engineering are depolarizing-fields effects and medium-driven interactions between dots. Interestingly, our findings may result in promising applications using negative refraction materials²⁰, nanomemory devices, etc.... They should also be relevant to, and thus lead to revisiting the analysis of, samples (i) made of composites²¹; (ii) in which segregation takes places (e.g., Ba(Zr,Ti)O₃ for intermediate compositions²²); (iii) in which chemically-ordered nanoregions form inside a disordered matrix (e.g., relaxors such as Pb(Mg,Nb)O₃²³). One can also easily imagine that further considering multi-component (e.g., three-component) systems can lead to even richer phase diagrams. Furthermore, designing some specific *lattice* of ferroelectric dots (inside some medium) may lead to other exotic states – as similar to the recent finding of Ref.²⁴ for nanoscale ferromagnetic islands.

We thank Igor Kornev for useful discussions. This work is mostly supported by DOE grant DE-FG02-05ER46188. We also acknowledge support from ONR grant N00014-04-1-0413 and NSF grant DMR-0404335. Some computations were made possible thanks to the MRI Grant 0421099 from NSF. S.P. also thanks RFBR grants 01-02-629&05-02-90568_HHC.

¹ J. F. Scott, *Ferroelectric Memories* (Springer-Verlag, Berlin, 2000).

² I. Naumov, L. Bellaiche and H. Fu, *Nature* **432**, 737 (2004).

³ I. Ponomareva, I. I. Naumov, I. Kornev, Huaxiang Fu, and L. Bellaiche, *Phys. Rev. B* **72**, 140102(R) (2005); I. Ponomareva, I. I. Naumov, and L. Bellaiche, *Phys. Rev. B* **72**, 214118 (2005).

⁴ H. Fu and L. Bellaiche, *Phys. Rev. Lett.* **91**, 257601 (2003).

⁵ V. M. Dubovik, M. A. Martsenyuk and N. M. Martsenyuk, *JMMM* **145**, 211 (1995).

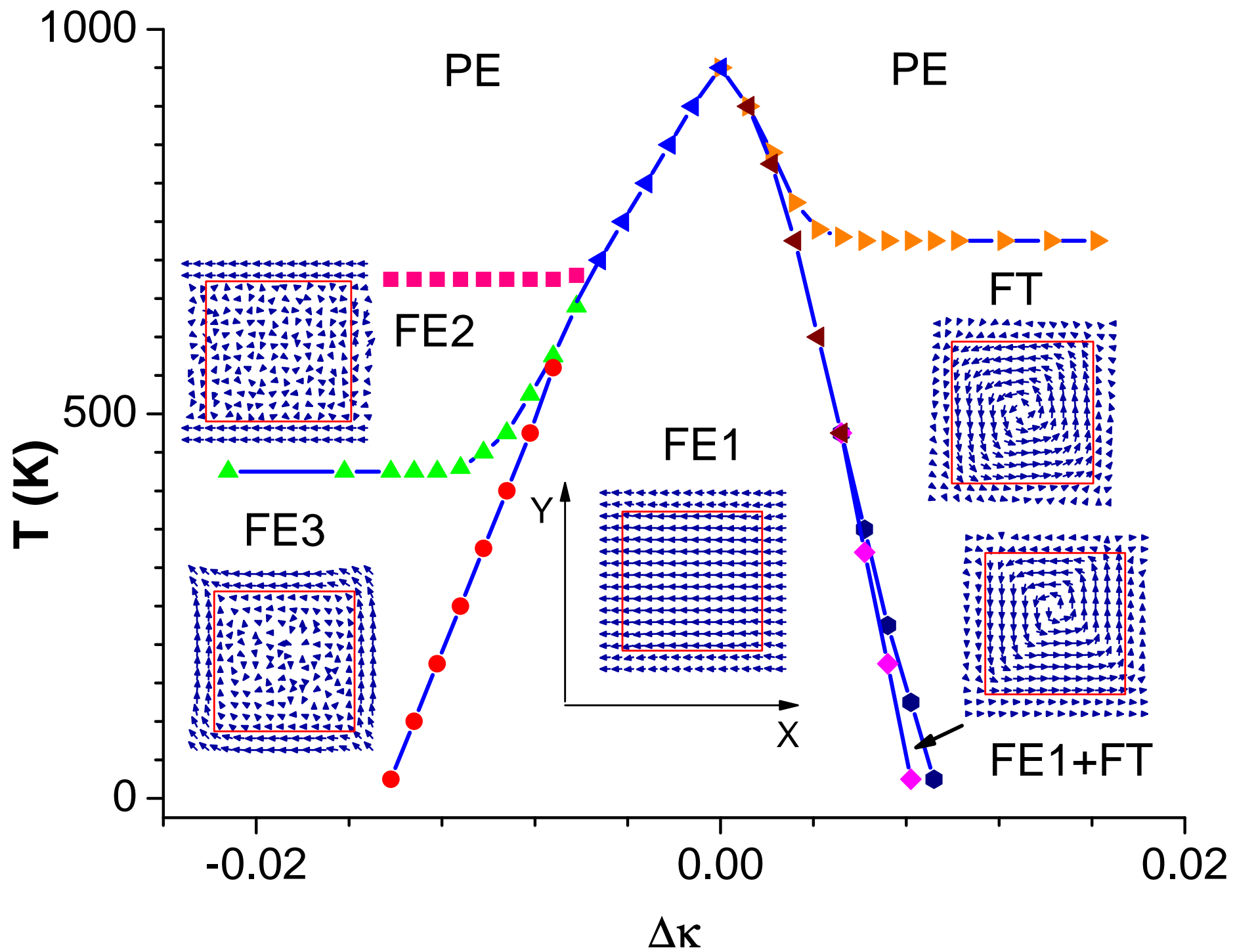
⁶ P. S. Neelakantaswamy, B. V. R. Chowdari and A. Rajaratnam, *J. Phys. D: Appl. Phys.* **16**, 1785 (1983).

- ⁷ Z.-M. Dang, Y. Shen, and C.-W. Nan, Appl. Phys. Lett. **81**, 4814 (2002).
- ⁸ G. Lim, J. Osman, and D. R. Tilley, Ferroelectrics **255**, 59 (2001).
- ⁹ L. Bellaiche, A. García and D. Vanderbilt, Phys. Rev. Lett. **84**, 5427 (2000); Ferroelectrics **266**, 41-56 (2002).
- ¹⁰ R. Hemphill, L. Bellaiche, A. García and D. Vanderbilt, Appl. Phys. Lett. **77**, 3642 (2000).
- ¹¹ L. Bellaiche and D. Vanderbilt, Phys. Rev. B **61**, 7877 (2000).
- ¹² W. Zhong, D. Vanderbilt and K.M. Rabe, Phys. Rev. Lett. **73**, 1861 (1994); Phys. Rev. B **52**, 6301 (1995);
- ¹³ C. Bungaro and K.M. Rabe, Phys. Rev. B **65**, 224106 (2002).
- ¹⁴ A. A. Gorbatsevich and Yu. V. Kopaev, Ferroelectrics **161**, 321 (1994).
- ¹⁵ A. García and D. Vanderbilt, in *First-Principles Calculations for Ferroelectrics: Fifth Williamsburg Workshop*, R.E. Cohen, ed. (AIP, Woodbury, New York, 1998), p. 53; Appl. Phys. Lett. **72**, 2981 (1998).
- ¹⁶ K. Binder, *Z. Phys. B* **43**, 119 (1981).
- ¹⁷ K. Yu. Guslienko, Appl. Phys. Lett. **78**, 3848 (2001).
- ¹⁸ S. Prosandeev, I. Ponomareva, I. Kornev, I. Naumov, and L. Bellaiche, Phys. Rev. Lett. **96**, 237601 (2006).
- ¹⁹ L. J. Heyderman, F. Nolting, D. Backes, S. Czekaj, L. Lopez-Diaz, M. Kläui and U. Rüdiger, C. A. F. Vaz, J. A. C. Bland, R. J. Matelon, U. G. Volkmann, and P. Fischer, Phys. Rev. B **73**, 214429 (2006).
- ²⁰ I. B. Vendik, O. G. Vendik, M. S. Gashinova, Tech. Phys. Lett. **32**, 429 (2006).
- ²¹ C. Huber, M. Treguer-Delapierre, C. Elissalde, F. Weill, and M. Maglione, J. Mater. Chem., **13**, 650 (2003).
- ²² R. Farhi, M. El Marssi, A. Simon, and J. Ravez, Eur. Phys. J. B **9**, 599 (1998).
- ²³ M. A. Akbas, and P. K. Davies, J. Phys. Chem. Solids **61**, 159 (2000).
- ²⁴ R. F. Wang, C. Nisoli, R. S. Freitas, J. Li, W. McConville, B. J. Cooley, M. S. Lund, N. Samarth, C. Leighton, V. H. Crespi, and P. Schiffer, Nature **439**, 303 (2005).

CAPTIONS

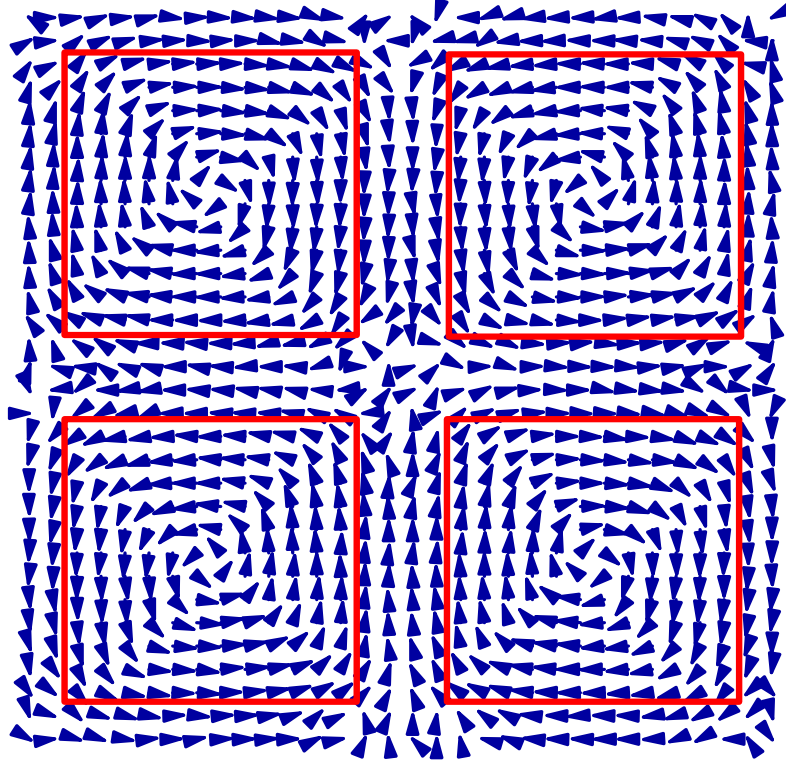
Fig. 1. Temperature-versus- $\Delta\kappa$ phase diagram of a $12 \times 12 \times 12$ $AB''O_3$ dot embedded in a $AB'O_3$ medium within a $16 \times 16 \times 16$ periodic supercell. The positive $\Delta\kappa$ part of this diagram corresponds to a soft ferroelectric dot immersed in a medium that is ferroelectrically harder than the dot and that has a decreasing ferroelectric instability as $\Delta\kappa$ increases. The negative $\Delta\kappa$ part of this diagram corresponds to a dot (having a ferroelectric instability that is weaker than those of the medium and that decreases, and then vanishes, as $\Delta\kappa$ increases in magnitude) embedded in a ferroelectrically-soft medium. The lines with symbols represent the phases' boundaries. The insets show a (001) cross-section of the dipole configuration in the different phases. Specifically, these insets correspond to atomistic calculations with the following $(\Delta\kappa, \text{temperature})$ combination: $(-0.0212 \text{ a.u.}, 1\text{K})$, $(-0.0212 \text{ a.u.}, 500\text{K})$, $(0.0062 \text{ a.u.}, 1\text{K})$, $(0.0087 \text{ a.u.}, 1 \text{K})$ and $(0.0112 \text{ a.u.}, 1\text{K})$ for the FE3, FE2, FE1, FE1+FT and FT phases, respectively. The dot surfaces are indicated via thick continuous lines in these insets. The x- and y-axes are chosen along the pseudo-cubic [100] and [010] directions, respectively.

Fig. 2. (001) cross-sections of the dipole configuration in the AFT and FE1+AFT phases in panels a and b, respectively, for four $12 \times 12 \times 12$ $AB''O_3$ dots embedded in a $AB'O_3$ medium within a $32 \times 32 \times 32$ periodic supercell. Such cross-sections specifically correspond to atomistic calculations for which the $(\Delta\kappa, \text{temperature})$ combination is $(0.0112 \text{ a.u.}, 1\text{K})$ and $(0.0087 \text{ a.u.}, 1\text{K})$ for the AFT and FE1+AFT states, respectively. The dots surfaces are represented by thick continuous lines. The x- and y-axes are chosen along the pseudo-cubic [100] and [010] directions, respectively.



AFT

a



FE1+AFT

Y

b

